[American Journal of Science, Vol. 307, December, 2007, P. 1146–1166, DOI 10.2475/10.2007.02]

APPLICABILITY OF AVERAGED CONCENTRATIONS IN DETERMINING GEOCHEMICAL REACTION RATES IN HETEROGENEOUS POROUS MEDIA

LI LI*,†, CATHERINE A. PETERS**, and MICHAEL A. CELIA**

ABSTRACT. This work examines the applicability of averaged concentrations, a mathematical analog of field-measured solute concentrations averaged over a large number of pores, in determining mineral reaction rates in heterogeneous porous media. Pore-scale network models were used to represent sandstones with anorthite and kaolinite as reactive minerals that are heterogeneously distributed in space. Reaction rates calculated from averaged concentrations were compared to true reaction rates that take into account variabilities in individual pore properties. Simulations were run under the highly acidic conditions relevant to geological CO_2 sequestration in deep brine formations under various mineralogical and flow conditions. Results show that, under conditions where incomplete mixing arises, the averaged concentrations and analogously the field-measured concentrations, do not accurately reflect reaction progress. Over the length scale of several millimeters, the anorthite dissolution rates can be overestimated by a factor of three. For kaolinite, due to its highly nonlinear reaction rate law, even the reaction direction may be incorrectly determined, with precipitation predicted as dissolution. The extent of errors introduced depends on the extent of incomplete mixing. Conditions that homogenize the concentration fields, such as small reactive mineral clusters, abundant reactive minerals, and very fast or very slow flow rates, minimize errors introduced from averaging. These results indicate that the averaging scheme may partly contribute to the often-cited laboratory-field rate discrepancy and have important implications for the interpretation of concentration data obtained from field investigation.

INTRODUCTION

Mineral reaction rates observed in natural settings are usually inferred from solute concentrations of field samples (Plummer and others, 1983; Parkhurst and Plummer, 1993; White and others, 1998; Yang and others, 2004; Zhu, 2005). These rates have been consistently found to be orders of magnitude smaller than those measured in laboratory systems. A multitude of factors have been considered to contribute to this often-cited rate discrepancy, including, for example, the differences in reactive surface areas of the freshly crushed minerals in laboratories and those of the weathered minerals in natural systems (Anbeek, 1993; Brantley and Velbel, 1993; White, 1995), the age of reacting minerals (White and Brantley, 2003; Maher and others, 2004), hydrologic controls, especially the amount of minerals in direct contact with flowing fluid (Parnell and Roderic, 1993; Swoboda-Colberg and Drever, 1993; Velbel, 1993), and the growth of secondary minerals on reacting surfaces (Steefel and Van Cappellen, 1990; Casey and others, 1993; Alekseyev and others, 1997).

Recent studies have also shown that the characteristics of natural porous media and flow conditions can play an important role in determining geochemical reaction rates in the field (Malmstrom and others, 2000; Mo and Friedly, 2000; Malmstrom and others, 2004; Li and others, 2006; Meile and Tuncay, 2006; Li and others, 2007a). For example, our previous work has shown that the heterogeneities of porous media, especially the mineral spatial distributions, can lead to spatial variations in concentra-

*Earth Sciences Division, Lawrence Berkeley National Laboratory, 1 Cyclotron Road, MS 90-1116, Berkeley, California 94720

**Department of Civil and Environmental Engineering, Princeton University, Princeton, New Jersey 08544

†Corresponding author: Li Li, lili@lbl.gov

tions — the concentrations at locations close to reacting surfaces can be very different from those at locations not in direct contact of reacting surfaces (Li and others, 2006, 2007a). One problem that arises from such conditions is that the field-measured solute concentrations, which are often drawn from a large number of pores and are essentially averaged concentrations (Appelo and Postma, 1996), may not represent the concentrations in the immediate vicinity of the reactive surfaces where reactions actually occur and may not accurately represent the reaction progress. Nonetheless, these "averaged" concentrations are often used to infer reaction rates in the field. As a result, such reaction rates may not accurately represent the reaction thermodynamics and kinetics in the field and may partly contribute to the observed rate discrepancy.

In fact, errors introduced in using averaged concentrations have been observed in recent studies. From both experimental (Kapoor and others, 1997, 1998; Raje and Kapoor, 2000; Gramling and others, 2002) and numerical studies (Kapoor and others, 1997), researchers have found that heterogeneities in flow fields produce spatial variations in concentrations and the use of averaged concentrations can erroneously predict reaction rates even for simple bimolecular reactions. Martin-Hayden and Robbins (1997) observed that averaged contaminant concentrations obtained from groundwater monitoring wells can predict distorted contaminant plumes and apparent attenuation that do not really exist. Molz and Widdowson (1988) reported that averaged oxygen concentrations can predict anaerobic conditions in what are actually aerobic zones. These observations document the effects of spatial heterogeneities at a large spatial scale and underscore the general principle that errors can be introduced when interpreting spatially-averaged concentrations measured in natural porous media.

This work extends our previous work by addressing the applicability of averaged concentrations (and by deduction, field-measured concentrations) in determining rates of mineral reactions that occur in natural porous media under various mineralogical and hydrodynamic conditions. This work continues to use the pore-scale network models developed for our previous study to represent sandstones with hypothetical, but realistic, pore-structures and mineral distributions (Li and others, 2006, 2007a). Detailed distributions and heterogeneities of pore structure and characteristics are explicitly taken into account in modeling the transport and reaction processes in individual pores so that the resulting concentration fields and reaction rates are affected by the heterogeneities of porous media. The reaction rates calculated based on the mass balance of such network systems represent the "true" reaction rates. They are compared to rates that are calculated using averaging assumptions to quantify the extent of error that can be introduced during averaging.

This work differs from our previous study in terms of the averaging schemes and meanings of the averaged reaction rates. In our previous studies, the averaging scheme used the well-mixed assumption *a priori* to average the porous medium properties before reactive transport modeling. As such, the averaged reaction rates represent those using the continuum approach in one grid block in forward modeling (Lichtner, 1985). In this work, the flux-averaging scheme is used *a posteriori* to represent the mixing processes in a well during field sampling. As such, the reaction rates calculated using the averaged concentrations represent those calculated from concentrations of field samples. The comparison between rates calculated from the flux-averaged concentrations and those without averaging therefore represent the errors that can be introduced in using averaged concentration in field samples. Quantifying these potential errors can be critical due to the ubiquitous use of the field samples not only in estimating mineral reaction rates in the field, but also in quantifying geochemical conditions for many important environmental problems, including, for example, radionuclide bioremediation (Anderson and others, 2003), organic contaminant

bioremediation (Zachara and others, 2004) and denitrification (Postma, 1990; Postma and others, 1991).

The network models constructed for this work simulated sandstones containing anorthite and kaolinite. These minerals are potentially relevant to geological CO_2 sequestration (Gaus and others, 2005; White and others, 2005) and long-term regulation of atmospheric CO_2 concentrations (Walker and others, 1981; White and Brantley, 1995). Anorthite is an important end member of the feldspar solid solution that can sequester CO_2 as carbonate mineral (Walker and others, 1981; Berner and others, 1983; White and Brantley, 1995). The anorthite reaction is as follows:

$$CaAl_2Si_2O_8(s) + 8H^+ = Ca^{2+} + 2Al^{3+} + 2H_4SiO_4. \quad (1)$$

Kaolinite has the following reaction:

$$Al_2Si_2O_5(OH)_4(s) + 6H^+ = 2Al^{3+} + 2H_4SiO_4 + H_2O. \quad (2)$$

To allow for the comparison with our previous work for the effects of different averaging schemes, the simulation conditions were chosen to be the same as in our previous study under temperature (323 K), pressure (10^7 Pa), and salinity conditions relevant to geological CO_2 sequestration (Li and others, 2007b). In addition, we look at the effect of flow conditions to identify the hydrodynamic conditions under which the introduced errors reach a maximum. Thirty-three pore-scale network models were simulated to investigate the effect of variations in mineral spatial distribution and abundance. For the influence of hydrodynamic conditions, eighteen different flow rates covering five orders of magnitude were examined.

METHODS

Pore-scale network modeling has been widely used in investigating transport phenomena in porous media, including multiphase flow (Celia and others, 1995; Blunt, 2001), drying processes (Prat, 2002), bubble transport (Stark and Manga, 2000), and in chemical and biological processes such as the dissolution of organic contaminants (Jia and others, 1999) and biomass growth (Suchomel and others, 1998). Pore-scale network models represent the porous media as an interconnected network of pores with various physical and chemical properties. At the pore network scale it maintains the continuum-scale characteristics of porous media, such as the porosity, permeability, and total amount of mineral surface area. It also takes into account details at the pore scale, including pore volume, pore surface area, *et cetera*. This modeling approach provides a useful means of studying averaging effects because concentrations and reaction rates at the pore network scale are related to concentrations and reaction rates at the scale of individual pores, a scale at which reaction processes are well-defined. Figure 1 shows a simplified schematic representation of a pore network model, although the network used in this work is of irregular shape, with no distinction between pore bodies and pore throats. This section briefly presents the pore-scale network modeling approach used in this work, calculation of continuum-scale reaction rates, and simulation conditions. More details are documented in Li and others (2006).

Network Construction

The constructed regular-latticed 3D network models correspond to a physical size of $3.4 \times 3.4 \times 3.4$ mm^3, each containing 8000 pores ($20 \times 20 \times 20$). The size of the networks is larger than the typical size defined by a Representative Elementary Volume (REV) (Li and others, 2007a), the volume at which the porous medium properties at the continuum scale can be defined (Bear, 1972). The properties of the networks, such as the porosity and the mineral surface area to volume ratio, stabilize when the number

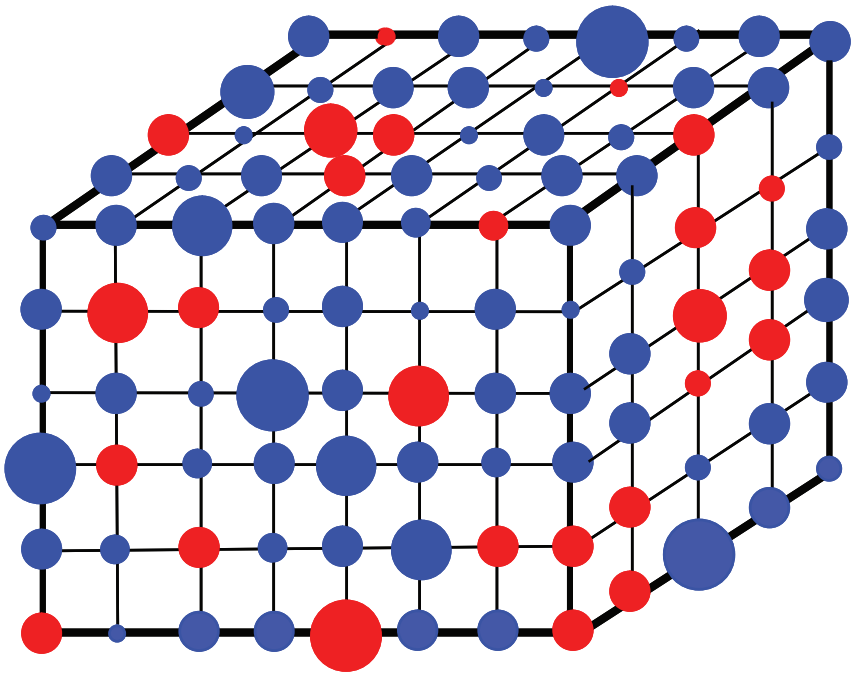

Fig. 1. A simplified conceptual representation of the pore-scale network model with pores of different volumes. The pores used in this work are actually of irregular shape, with no distinction between pore bodies and pore throats. The red color indicates reactive pores and the blue color represents non-reactive pores.

of the pores exceeds 6000 (Li and others, 2007a). As such, the continuum scale is defined here to refer to the scale of the entire network of pores. At this scale, the network models have physical properties of typical consolidated sandstone, with a porosity of 0.14, a surface area to volume ratio of 1.3×10^{4} cm^{-1}, and a permeability of 7.9×10^{-10} cm^{2} (79 milliDarcy). Within the network, each pore is characterized by several parameters, including pore volume, pore-to-pore hydraulic conductance, pore surface area, and pore-to-pore cross-sectional surface area. Across the network each parameter forms a statistical distribution, from which the parameters for individual pores are randomly sampled. The form and the parameters for each distribution are based on literature data for consolidated sandstones (Freeze, 1975; Wardlaw and others, 1987; Sen and others, 1990; Lymberopoulos and Payatakes, 1992; Borgia and others, 1996; Turcke and Kueper, 1996; Frosch and others, 2000; Lindquist and others, 2000; Ross, 2000), as listed in table 1.

To model uneven spatial distribution of minerals in sedimentary rocks (Carozzi, 1993), pores are classified as either non-reactive, that is, containing only quartz, or as reactive, with anorthite and kaolinite each occupying half of the solid. This classification is based on the fact that the quartz reaction rate is more than six orders of magnitude smaller than the anorthite and kaolinite reaction rates under the same conditions (Kump and others, 2000). Such formulation allows kinetic reactions to occur only in reactive pores, which is accurate for dissolution reactions, but is not necessarily the case for precipitation reactions. This can be justified by the fact that in non-reactive pores, precipitation reactions would need to go through a nucleation step before crystal growth due to the lack of reactive mineral surface area. Because the nucleation step is often the rate-limiting step (Steefel and Van Cappellen, 1990;

Table 1

Parameters for the statistical distributions of the network properties

Parameters	Form of distribution	mean	variance
Pore volume [a]	Lognormal	-3.42 mm^3	0.51
Pore surface area [b]	Exponential	6.0 mm^2	———
Pore conductance [c]	Lognormal, conditioned on connected pore volumes	-6.1 cm^4 g Pa^{-1}	1.0
Pore cross-sectional area	Calculated from pore conductance	1.02×10^{-4} mm^2	———

a. Based on Lindquist and others (2000).
b. Based on Sen and others (1990), Borgia and others (1996), and Frosch and others (2000).
c. Based on Freeze (1975), Lymberopoulos and Payatakes (1992), Wardlaw and Forbes (1987), and Ross (2000).

Lasaga, 1998; Giammar and others, 2005), the precipitation reaction would occur much more slowly in non-reactive pores than in reactive pores, so that within the short time frame considered in this work, this effect is assumed to be negligible. With longer time frames, however, precipitation will gradually occur and reactive mineral surface area will accumulate in non-reactive pores, and the inclusion of precipitation in non-reactive pores may become necessary.

Given a fixed total amount of reactive minerals for the network, reactive pores are organized in randomly-distributed uniformly-sized cubic clusters. The size of the pore clusters is defined by the cluster length and the number of pores in one dimension. To examine the effects of reactive cluster size, network models were constructed with reactive clusters of size ranging from a length of one to a length of sixteen. In the cases of all reactive pores gathered in one single cluster, the reactive cluster is positioned in the center of the network. The effects of reactive mineral abundance were examined with the percentage of reactive minerals being 6.25 percent, 12.5 percent, 25 percent, and 50 percent. For each case, four realizations were simulated by keeping the bulk properties constant at the network scale. That is, the porosity, permeability, reactive mineral cluster size and abundance were kept constant for each realization, while the parameters of individual pores were randomly assigned and can vary from one realization to another. The results from the four realizations, such as values of continuum-scale reaction rates, were averaged to represent the rates for each case and the range of the values are represented with bars.

Pore-Scale Modeling of Reactive Transport Processes

The steady-state flow field was determined before the pore-scale reactive transport simulation. In this work we assign pressure gradients at the boundaries in one direction, with all other boundaries as no flow boundary. This results in macroscopically one dimensional flow. The flow rate between pore i and its neighbor pore j is proportional to the conductance and pressure difference between the two pores. For each pore i, the inflow and outflow must be balanced. That is,

$$\sum_{j=1}^{nc} Q_{ij} = 0. \tag{3}$$

Here nc is the total number of pores connected to pore i (normally six); Q_{ij} symbolizes the flow rate between pore i and j. For each pair of connected pores, the direction of the flow is opposite so that $Q_{ij} = -Q_{ji}$. As such, the flows within the network are

TABLE 2

Reactions included in reactive transport modeling, with equilibrium constants adjusted to simulation conditions at 50 degree C and 100 bars

	Reactions	$\log K_{eq}$ [a]
Kinetic reactions	$CaAl_2Si_2O_8(s)+8H^+ = Ca^{2+}+2Al^{3+}+2H_4SiO_4$	21.7
	$Al_2Si_2O_5(OH)_4(s) + 6H^+ = 2Al^{3+}+2H_4SiO_4+H_2O$	3.80
Instantaneous reactions	$H_2O = H^+ + OH^-$	-13.2
	$H_2CO_3^* = H^+ + HCO_3^-$	-6.15
	$HCO_3^- = H^+ + CO_3^{2-}$	-10.0
	$H_4SiO_4 = H^+ + H_3SiO_4^-$	-9.2
	$H_3SiO_4^- = H^+ + H_2SiO_4^{2-}$	-12.4
	$Al^{3+} + OH^- = Al(OH)^{2+}$	8.76
	$Al^{3+} + 2OH^- = Al(OH)_2^+$	18.9
	$Al^{3+} + 3OH^- = Al(OH)_3$	27.3
	$Al^{3+} + 4OH^- = Al(OH)_4^-$	33.2
Species Involved	H^+, OH^-, Ca^{2+}, Al^{3+}, $Al(OH)^{2+}$, $Al(OH)_2^+$, $Al(OH)_3$, $Al(OH)_4^-$, H_2CO_3, HCO_3^-, CO_3^{2-}, H_4SiO_4, $H_3SiO_4^-$, $H_2SiO_4^{2-}$	
Components or total species[b]	$[Ca_T] = [Ca^{2+}]$ $[C_T] = [H_2CO_3^*] + [HCO_3^-] + [CO_3^{2-}]$ $[Si_T] = [H_4SiO_4] + H_3SiO_4^- + H_2SiO_4^{2-}$ $[Al_T] = [Al^{3+}] + [Al(OH)^{2+}] + [Al(OH)_2^+] + [Al(OH)_3] + [Al(OH)_4^-]$ $[H_T] = -[Al(OH)^{2+}] - 2[Al(OH)_2^+] - 3[Al(OH)_3] - 4[Al(OH)_4^-] + [H_4SiO_4] + [H_3SiO_4^-] - [H_2SiO_4^{2-}] + [H_2CO_3^*] - [CO_3^{2-}] + [H^+] - [OH^-]$	

a. Equilibrium constants were taken from Morel and Hering (1993) and adjusted to the system temperature and pressure using SUPCRT (Johnson and others, 1992).
b. The components or total species are defined using the formulation of Lichtner (1985) or the tableau method introduced in Morel and Hering (1993).

cancelled out. Therefore, the overall flow rate for the network, which is the summation of flow of all pores, is equal to the summation of flow rates that enters or leaves the network.

The relevant reactions include anorthite and kaolinite reactions, which are considered kinetically, and nine additional instantaneous aqueous reactions, as listed in table 2. In total 14 relevant species are considered. Time scale analysis has shown that the mass transport (diffusion and advection) is relatively fast compared to chemical kinetics at the spatial scale of individual pores (Li and others, 2006). As such, concentration gradients are small and we can assume spatially uniform concentrations within individual pores. In other words, we do not need to discretize further within a pore. Within each pore, the mass change of chemical species is described by mass balance equations, developed following Lichtner's systematic formulation (Lichtner, 1985). With this formulation, the mass balance equations for our interested system can

be written for five components, or total species, that are linear combination of the 14 aqueous species, as listed in table 2. The mass balance equations describe mass change rates due to advection, diffusion between adjacent pores, and reactions, and take the following general form (for pore i):

$$V_i \frac{d[\bullet]_i}{dt} = \sum_{\substack{j=1 \\ Q_{ij}>0}}^{nc} Q_{ij}[\bullet]_j + \sum_{\substack{j=1 \\ Q_{ij}<0}}^{nc} Q_{ij}[\bullet]_i + \sum_{j=1}^{nc} D^*_{\bullet,ij} a_{ij} \frac{([\bullet]_j - [\bullet]_i)}{l} + S_{\bullet,i} \tag{4}$$

where [•] represents the concentration of one of the components; V_i is the volume of pore i; j is the index for the pores that are connected to pore i; $D^*_{\bullet ij}$ is the effective diffusion coefficient of the component between pore i and its neighbor pore j, which depends on the local concentration gradients of the component between pore i and pore j; a_{ij} is the cross-sectional area between pore i and j; l is the distance between centroids of connected pores; and $S_{\bullet,i}$ denotes the mass change rate due to kinetic reactions.

The values of $D^*_{\bullet,ij}$ for the collective components were calculated based on the species-dependent diffusion coefficients. For example, for total carbonate C_T, the diffusion coefficient is calculated as follows:

$$D^*_{C_T,ij} = \frac{D_{H_2CO_3^*}([H_2CO_3^*]_j - [H_2CO_3^*]_i) + D_{HCO_3^-}([HCO_3^-]_j - [HCO_3^-]_i) + D_{CO_3^{2-}}([CO_3^{2-}]_j - [CO_3^{2-}]_i)}{([H_2CO_3^*]_j - [H_2CO_3^*]_i) + ([HCO_3^-]_j - [HCO_3^-]_i) + ([CO_3^{2-}]_j - [CO_3^{2-}]_i)} \tag{5}$$

Such calculation does not take into account the electrochemical migration arising from a diffusion potential caused by the different diffusion rates of charged species (Newman, 1991). Under conditions relevant to geological CO_2 sequestration, however, the ubiquitous presence of the high background salinity diminishes this effect (Giambalvo and others, 2002; Li and others, 2007a). This formulation also explicitly incorporates the spatial variability in pore-scale flow rates, which generates a dispersion effect at the continuum scale.

The reaction term, $S_{\bullet,i}$, for each component in each pore is the sum of the rates of all of the involved kinetic reactions. The rate of each kinetic reaction in pore i is the product of the area-normalized reaction rate and its surface area in that pore A_i. As such, the anorthite and kaolinite reaction rates in individual pores, $r_{A,i}$ and $r_{K,i}$ (mol cm^{-2} s^{-1}), respectively, are calculated using their respective reaction rate laws and the local concentrations (Lasaga, 1998). Under the highly acidic conditions of interest in this work, the anorthite reaction rate in pore i is calculated as follows:

$$r_{A,i} = k_H \{H^+\}_i^{n_H} (1 - \Omega_{A,i}), \tag{6}$$

with the following expression for the saturation state

$$\Omega_{A,i} = \frac{\{Ca^{2+}\}_i \{Al^{3+}\}_i^2 \{H_4SiO_4\}_i^2}{\{H^+\}_i^8 K_{eq,A}}. \tag{7}$$

Here, k_H is the reaction rate constant, with a value of $10^{-7.07}$ mol cm^{-2} s^{-1} (Oelkers and Schott, 1995); n_H is a constant that describes the degree of catalytic effect of hydrogen ion activities, with a value of 1.5 (Oelkers and Schott, 1995); $\{\bullet\}_i$ indicates the activity of an aqueous species in pore i (mol/L); and $K_{eq,A}$ denotes the equilibrium constant of the anorthite reaction. Similarly, for the kaolinite reaction rate,

$$r_{K,i} = k_H\{\mathrm{H}^+\}_i^{n_H}(1 - \Omega_{K,i}^m), \tag{8}$$

with the following expression for

$$\Omega_{K,i} = \frac{\{\mathrm{Al}^{3+}\}_i^2\{\mathrm{H_4SiO_4}\}_i^2}{\{\mathrm{H}^+\}_i^6\mathrm{K}_{\mathrm{eq,K}}} \tag{9}$$

In this rate law, the value of k_H is $10^{-14.8}$ mol cm^{-2} s^{-1} (Ganor and others, 1995); the value of n_H is 0.4 (Ganor and others, 1995), and m is a constant that describes the degree of the dependence on the saturation state of the aqueous phase, with a value of 0.9 (Nagy and others, 1991). For example, for the species Ca^{2+}, the reaction term is calculated as the following:

$$S_{\mathrm{Ca}^{2+},i} = A_{A,i}r_{A,i} \tag{10}$$

Due to the heterogeneous nature of the network, the parameters in equation (4), including the pore volume and surface areas of reacting surfaces vary from pore to pore. Parameters such as conductance, diffusion coefficients, the cross-sectional area are different not only from pore to pore, but also for each connection to neighbor pores for each pore *i*. The reactive transport equation (4), coupled with laws of mass action for instantaneous reactions, was used to solve concentrations of all fourteen species in each pore at each time step. Details of the numerical methods were documented in Li and others (2006).

Continuum-Scale Rates from the Network Model: R_N

The pore-scale reactive transport modeling above gives detailed information on the local concentrations and reaction rates in individual pores, based on which the overall reaction rates across the network can be calculated. The size of the computational domain, that is, the pore network, is chosen to be larger than the Representative Elementary Volume (Bear, 1972; Li and others, 2007a) so that the overall reaction rates at the pore network scale are continuum-scale reaction rates. The continuum-scale reaction rates can be calculated based on the mass balance of the network. The total mass change rate of the network is the summation of equation (4) for all pore *i*. For example, for total Ca^{2+}, this gives us the following:

$$\sum_{i=1}^{n} V_i\frac{d[\mathrm{Ca}^{2+}]_i}{dt} = \sum_{i=1}^{n}\sum_{\substack{j=1\\Q_{ij}>0}}^{nc} Q_{ij}[\mathrm{Ca}^{2+}]_j + \sum_{i=1}^{n}\sum_{\substack{j=1\\Q_{ij}<0}}^{nc} Q_{ij}[\mathrm{Ca}^{2+}]_i + \sum_{i=1}^{n}\sum_{j=1}^{nc} D^*_{\mathrm{Ca}^{2+},ij}a_{ij}\frac{([\mathrm{Ca}^{2+}]_j - [\mathrm{Ca}^{2+}]_i)}{l} + \sum_{i=1}^{n} A_{A,i}r_{A,i} \tag{11}$$

where n is the total number of pores. In this work, we consider reaction rates after the system reaches steady state, where concentrations in individual pores do not change as a function of time. As such, the left hand side of equation (11) becomes zero. At the right hand side, the flow terms within the network cancel out, except for the ones that enter and exit the network. These are the pores that directly connect to the boundary. The diffusion terms for all pores also cancel out due to the opposite directions of the concentration gradients between neighbor pores. As such, the overall reaction term $\sum_{i=1}^{n} A_{A,i}r_{A,i}$ is equivalent to the change in mass between outflow and inflow and is the net overall reaction rate across the network taking into account all available reacting surfaces. The area-normalized overall reaction rates are therefore calculated as the following for anorthite:

$$R_{N,A} = \frac{\sum_{i=1}^{n} A_{A,i} r_{A,i}}{\sum_{i=1}^{n} A_{A,i}} \tag{12}$$

The calculation of the continuum-scale rate for kaolinite ($R_{N,K}$) is analogous. This rate represents the "true" reaction rates for the network calculated from the mass balance of the network system and has explicitly taken into account the effect of pore-scale heterogeneity. Because reactions occur only in reactive pores that have non-zero values of surface area of anorthite and kaolinite, the continuum-scale dissolution rates are determined only by concentrations in reactive pores where kinetic reactions occur.

Continuum-Scale Rates from Averaged Concentrations: R_N'

During field sampling, water from a large number of pores enters the sampling well and is mixed within the well. The amount of water entering a sampling well from each pore is proportional to the flux out of the pore. The mixing process conserves the total mass of the components and imposes the requirement of homogeneous equilibria. To computationally represent this process, we use flux-weighted average concentrations to represent the concentrations of components measured from field samples. For example, for total calcium species, the average concentration $\overline{[Ca^{2+}]}$ is computed as follows:

$$\overline{[Ca^{2+}]} = \frac{\sum_{i=1}^{n} Q_{t,i}[Ca^{2+}]_i}{\sum_{i=1}^{n} Q_{t,i}} \tag{13}$$

where $Q_{,i}$ is the sum of fluxes either into or out of pore i. The flux-averaged concentrations of the other four components were calculated in the same way. With the flux-averaged concentrations of the total species, the laws of mass action for the nine instantaneous reactions were then imposed to obtain averaged concentrations of all fourteen species. For example, the averaged concentration of hydrogen ion is calculated based on speciation of the involved instantaneous reactions and the concentrations of the five components in the system. The averaged pH is then calculated as $pH = -\log_{10}\{H^+\}$. With the averaged concentrations of all 14 species, the continuum-scale rates, R_N', were then calculated using reaction rate laws expressed in equations (6) and (8). Reaction rates calculated from these concentrations are mathematical analogs to the spatially averaged rates calculated from measured concentrations from field samples.

The flux averaging procedure indiscriminately takes into account concentrations in all pores, including those in non-reactive pores that may not reflect reaction progress. The resulting concentrations may not accurately represent the concentrations at reactive sites in a heterogeneous porous medium, thereby serving as poor indicators of the overall reaction rates in the porous medium. However, such averaging procedure is done here on purpose to see how much error can be introduced in using these concentrations from field samples. Although this flux averaging is different from volume averaging, the resulting averaged concentrations actually are quite similar to volume-averaged concentration, as shown in another contribution (Li and others, 2007a). The flux-averaging approach is also a different approach for calculating the continuum-scale averaged reaction rates than what was used in our previous work that represent averaging assumptions used in forward modeling (Li and others, 2007a).

Comparison Between Continuum-Scale Reaction Rates

For the comparison of R_N' and R_N, we define the ratio:

$$\beta = \frac{R_N'}{R_N}, \tag{14}$$

and a subscript A or K is used to denote the values for anorthite and kaolinite, respectively. The deviation of the value from unity provides a measure of how well the rates based on averaged concentrations represent "true" reaction rates and the extent of error introduced in R_N'. Although this definition is similar to that of the η value defined in our previous work (Li and others, 2007b), the meaning of β is different in that it quantifies the difference between the rates calculated from flux-averaged concentrations and "true" reaction rates based on the mass balance of the network.

Simulation Conditions

The simulations were run under conditions relevant to geological sequestration of CO_2 in deep brine formations, at 323 K, 10^7 Pa, and total dissolved salinity of 0.45 mol/L as sodium chloride. Due to the high salinity, the activity coefficients were considered constant both in time and space and were estimated using the Davies equation (Morel and Hering, 1993). Equilibrium constants were taken from Morel and Hering (1993) and adjusted to the simulation conditions using the software SUPCRT (Johnson and others, 1992). Initially the brine is assumed to be in equilibrium with quartz and kaolinite at pH 7.5. The brine at the inflowing boundary is assumed to have the same $[Ca^{2+}]$ as in the initial aqueous phase within the network, with its total carbonate concentration calculated from phase equilibrium with carbon dioxide (Duan and Sun, 2003) at a pressure of 10^7 Pa, corresponding to a boundary pH of 2.9.

To examine the effects of variations in reactive mineral spatial distributions, the simulations were run for a flow velocity of 4.6×10^{-3} cm/s, which corresponds to conditions of proximity to an injection well (Knapp, 1989). In examining the effect of hydrodynamic conditions, the Darcy flow velocity at the pore network scale was varied from 10^{-5} to 10^2 cm/s. The systems were run until reaching steady state, where the concentrations of each species and reaction rates do not change with time. The actual time to reach steady state depends on the flow velocity, ranging from tens of thousands of seconds for a flow velocity of 10^{-5} cm/s to tens of seconds for a flow velocity of 10^2 cm/s. Due to the relatively slow rates of mass change in the solid phase compared to those in the aqueous phase, the change in porous medium properties (porosity, permeability, and mineral surface area) is negligible within the time frame to reach steady state. As such, the model assumes no change in porous media properties.

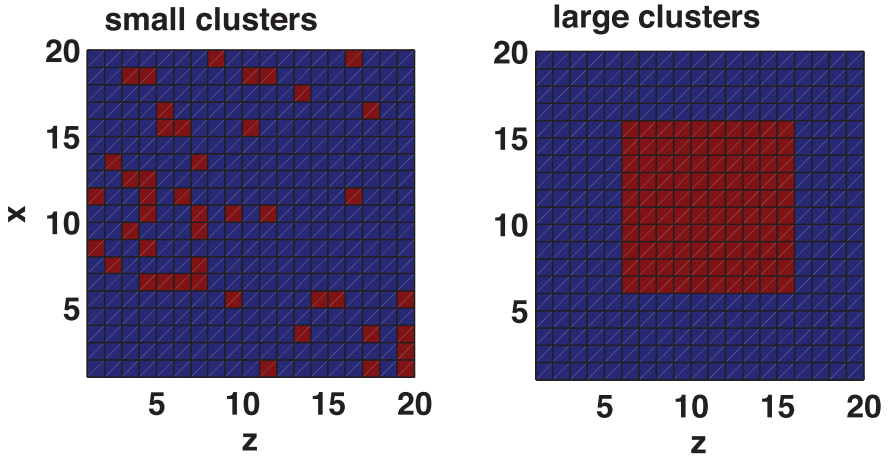

Fig. 2. 2D cross-sections of the pore network with small reactive clusters (left) and large reactive clusters (right). The red ones indicate reactive pores.

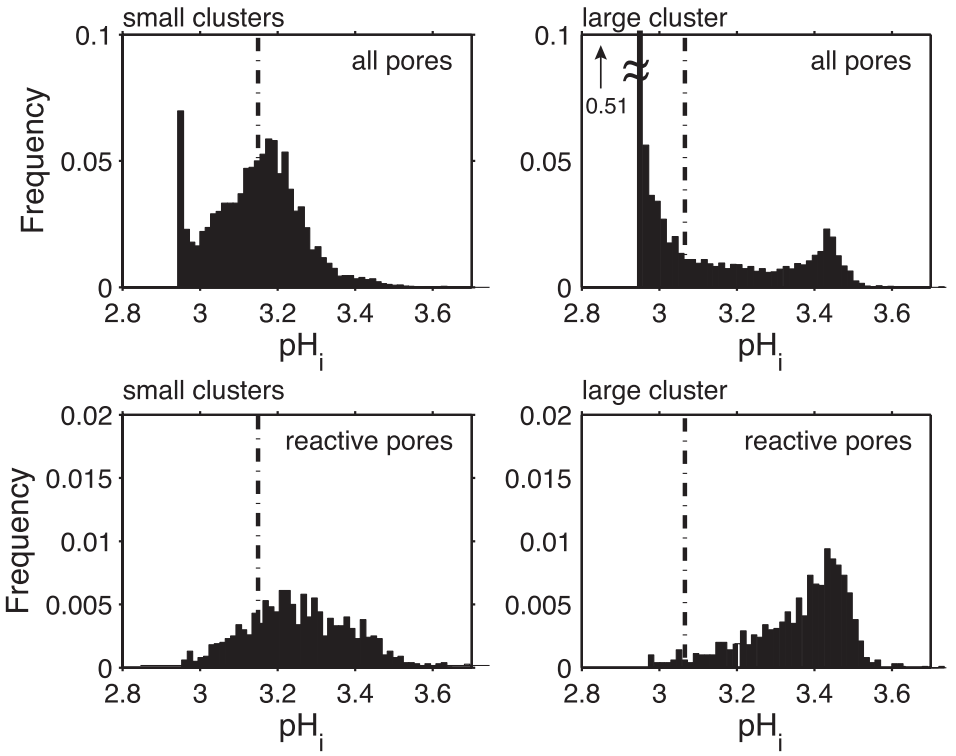

Fig. 3. Distribution of pH for networks with reactive clusters of small size (one pore) and of large size (a thousand pores) for all pores and for only reactive pores. The dotted-dashed lines indicate averaged pH values, calculated as $pH = -\log_{10}\{H^+\}$ using hydrogen ion activity obtained from the flux-averaged calculation and homogenous equilibria.

RESULTS

Effects of Reactive Cluster Size

Steady-state pH values and reaction rates are compared for two extreme cases: a network with the smallest clusters (cluster length being one), and one with a single large cluster that is ten pores in length. Figure 2 shows a 2D cross-section of the pore network for one realization for both cases. The total amount of reactive minerals is nominally 12.5 percent of the solid phase. The steady-state pH distributions for the two cases are shown in figure 3. For each case, the pH values are shown for all the pores in the network as well as for only the reactive pores. For both cases, hydrogen ion concentrations span 0.7 orders of magnitude, indicating large concentration gradients at the network scale. In general, the consumption of hydrogen ions due to anorthite dissolution produces higher pH values in reactive pores.

The size of reactive mineral clusters plays a large role in determining the concentration distributions. In the small cluster case, the distribution has a primary mode, with its value roughly the same as the mode of the distribution in reactive pores. In the large cluster case, however, the distribution across all pores is bimodal, with one mode being the value of the boundary pH and the other mode corresponding to the elevated pH values in reactive pores. Furthermore, in the large cluster case, there are more reactive pores with high pH values.

As discussed by Li and others (2006), such differences in the concentration distributions are due to the differences in mass transport between reactive and

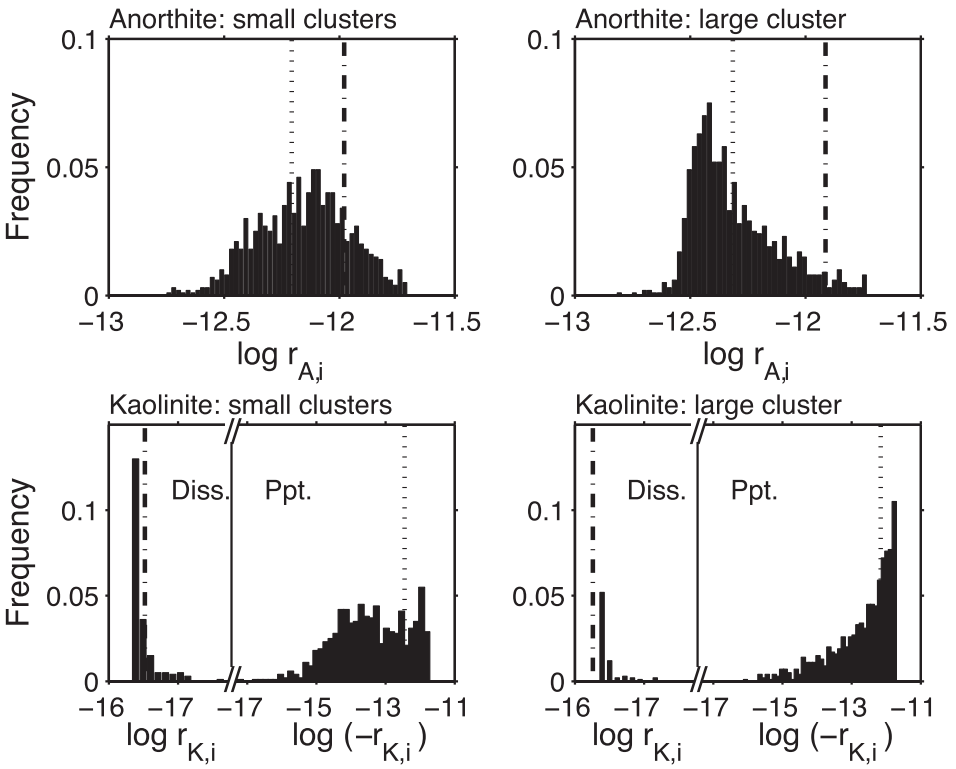

Fig. 4. Anorthite and kaolinite steady-state rate distributions for clusters of size one ("small") and a thousand ("large"). Rates are in units of mol cm^{-2} s^{-1}. In the kaolinite plots, two regions are shown: one showing the dissolution rates ("Diss") and one showing the precipitation rates ("Ppt"). The dotted lines indicate rates calculated from network modeling, R_N, and the dot-dashed lines indicate rates calculated from averaged concentrations, R_N'.

non-reactive pores, arising from the different sizes of reactive clusters. With small clusters, each reactive pore is in contact with several non-reactive pores, which favors the mass transport and leads to a more evenly distributed concentration field. With large reactive clusters, there are fewer interfaces between reactive and non-reactive pores, and concentrations in most non-reactive pores are not influenced by those in reactive pores.

Also shown in figure 3 are the averaged pH values, computed as $\text{pH} = -\log_{10}\{H^+\}$ using hydrogen ion activities obtained from the averaging calculation detailed in the previous section. For both cases, the averaged pH values overestimate the hydrogen ion concentrations in reactive pores. However, the extent of overestimation is much larger in the large cluster case, where the averaged pH is close to the boundary pH and hence represents the pH values in non-reactive pores.

Figure 4 shows the distributions of steady-state reaction rates in reactive pores in the network. In both cases, the anorthite rates span more than an order of magnitude. The shapes of the anorthite rate distributions are similar to their respective distributions of negative pH in reactive pores, illustrating the governing role that pH plays in controlling reaction kinetics. Also shown in the figure are the "true" rates calculated from the network modeling, R_N, and the rates calculated using the averaged concentrations, R_N'. Values of R_N are close to the modes of the rate distributions, while values of R_N' are farther from the peak and overestimate the actual reaction rates. As expected

from the pH distributions, the difference between the two rates is larger in the large cluster case.

For kaolinite, precipitation occurs in most pores, but dissolution occurs in some pores. In both small and large cluster cases, values of $R_{N,K}$ indicate overall precipitation, while values of $R_{N,K}'$ indicate kaolinite dissolution, which not only predicts the wrong reaction rates, but also the wrong reaction direction. Such a large error is primarily caused by flux averaging combined with the high sensitivity of the kaolinite reaction rate to pH. Combining equations (8) and (9) and considering $1 - \Omega_{K,i}^m \approx \Omega_{K,i}^m$ for precipitation, kaolinite precipitation rates depend on hydrogen ion concentration raised to the power of -5.0. With such high dependence, even small overestimation of hydrogen ion concentrations can lead to large errors in reaction rates. For anorthite dissolution, under highly acidic conditions, the reaction is far from equilibrium and the value of $1 - \Omega_{A,i}$ is essentially unity for all pores. As such, the rate depends only on hydrogen ion concentration raised to the power of 1.5 and the error introduced in $R_{N,A}'$ is relatively smaller.

Figure 5 shows R_N and R_N' versus cluster length for all the network simulations with 12.5 percent reactive mineral and hydrodynamic flow rate of 4.6×10^{-3} cm/s. Each data point is an averaged value from four realizations. The error bars are presented to see the magnitude of difference between different realizations. For anorthite dissolution, the network model predicts that the rate decreases with cluster length, due to the increasing number of pores with high pH, while R_N' predicts that rates increase with cluster size, due to the increasing overestimation of hydrogen ion concentration. As a result, the difference between these two rates increases with cluster size. For kaolinite, the network model predicts increasing precipitation rates with increasing cluster size, while R_N' predicts the opposite reaction direction, with rates that are orders of magnitude smaller than the precipitation rates.

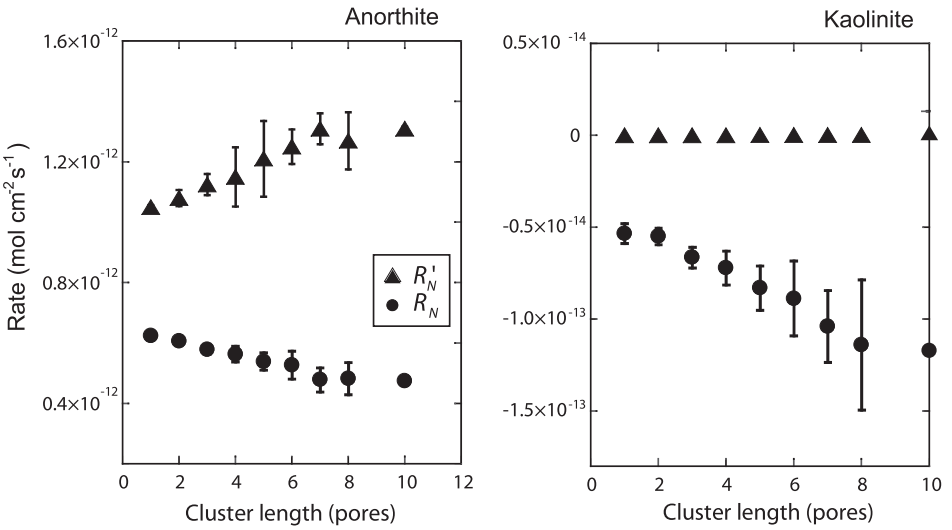

Fig. 5. Comparison of rates from the network model R_N and those from the averaged concentrations R_N' over a range of cluster lengths, for the case where reactive minerals occupy nominally 12.5%. The reaction rates were obtained by averaging over four realizations for each case. The error bars are presented to see the magnitude of differences between different realizations.

Effects of Reactive Mineral Abundance

To illustrate the effect of both reactive cluster size and reactive mineral abundance on differences between R_N and R_N', figure 6 shows β values as a function of cluster length, with reactive mineral abundance ranging from 6.25 percent to 50 percent. The simulations were conducted at the flow velocity of 4.6×10^{-3} cm/s, with cluster lengths ranging from one to sixteen. For a specific cluster size, β_A values increasingly deviate from unity with decreasing percentages of reactive minerals. For a specific reactive mineral abundance, the β_A values increase with cluster size, although the increase diminishes or even reaches a plateau with larger clusters. For kaolinite precipitation, in the case of 6.25 percent and 12.5 percent, β_K values are negative (although it is difficult to see this in figure 6 due to the small magnitude of the values); in the 25 percent and 50 percent case, β_K values are positive, indicating the correct prediction of reaction direction by $R_{N,K}'$. With increasing percentages of reactive mineral, the $R_{N,\,K}'$ value increasingly approaches the correct prediction of reaction direction; the β_K values are closer to unity, indicating the decreasing magnitude of errors.

Effects of Hydrodynamic Conditions

To illustrate the effect of hydrodynamic conditions, figure 7 shows continuum-scale steady-state rates of anorthite and kaolinite reactions for mean flow velocities varying from10^{-5} to10^{2} cm/s, for a pore network with clusters of four pores in length and with reactive mineral abundance of 12.5 percent. For the anorthite dissolution, both R_N and R_N' decrease with decreasing flow velocities, due to the reduced hydrogen ion concentrations as a result of prolonged reaction times to reach steady state. For the kaolinite reaction, R_N and R_N' show very different behavior. The precipitation rate from the network model (R_N) increases first and then decreases with decreasing flow velocities, while those from the averaging calculation (R_N') transit from dissolution to precipitation, with the precipitation rates increasing with decreasing flow velocities. For both anorthite and kaolinite reactions, the differences between R_N and R_N' show

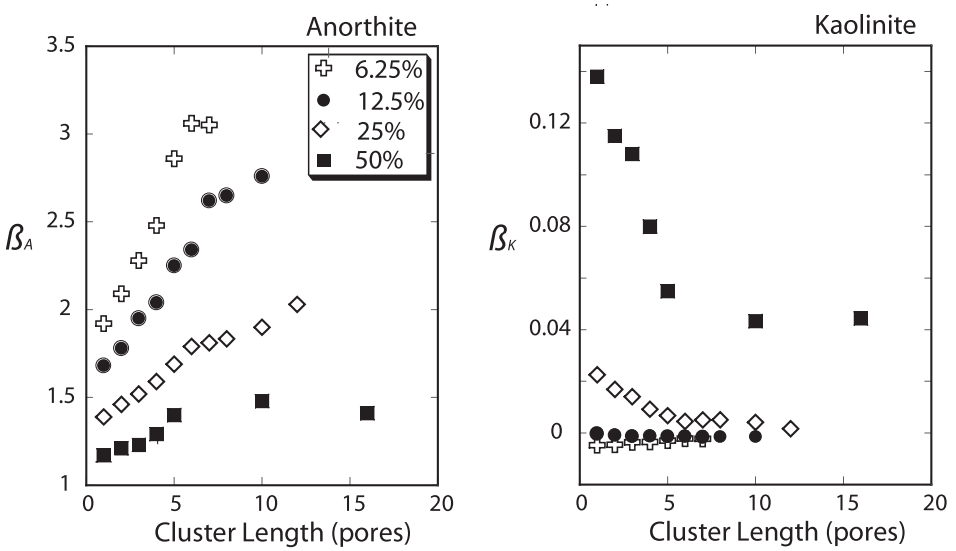

Fig. 6. Values of β for different cluster sizes for different percentages of reactive minerals. The β values were obtained by averaging over four realizations in each case.

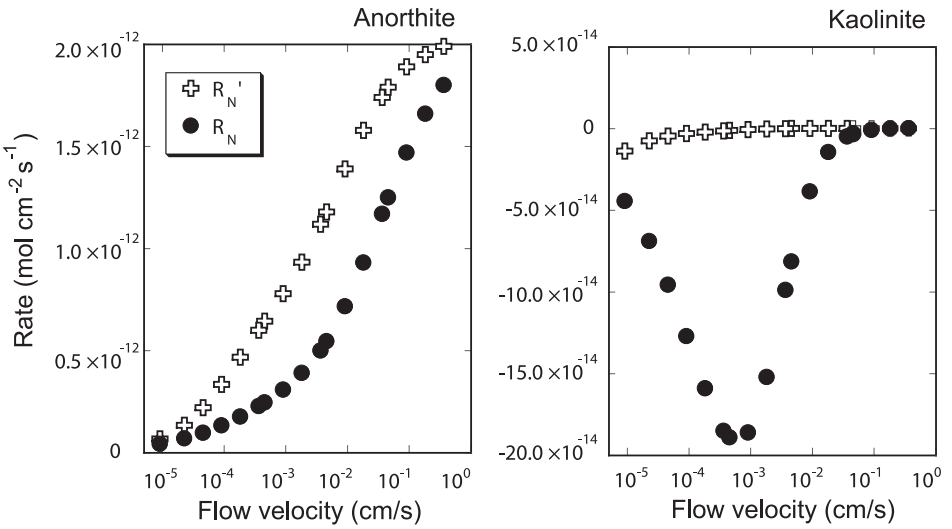

Fig. 7. For a reactive cluster size of four pores in length: values of R_N' and R_N under different hydrodynamic conditions, for anorthite and kaolinite reactions.

three distinct regions. With fast and slow flow velocities, the rates from the two models are similar; with medium flow velocities, the differences are the largest. For the kaolinite reaction, even the reaction direction cannot be correctly determined in the medium flow velocity region.

Such phenomena are a result of the relative importance of reaction and transport at different flow conditions and the resulting heterogeneities in the concentration field. Figure 8 illustrates the effects of variations in hydrodynamic conditions on steady-state pH profiles in a single network layer for a fast flow velocity of 3.6×10^{-2} cm/s and a medium flow velocity of 3.6×10^{-4} cm/s. Also shown is the distribution of reactive minerals in this layer. Variations in hydrodynamic conditions have a significant effect on concentration fields. With a high mean flow velocity, advection is much faster than reaction, and the residence time is small so pores are quickly flushed with fresh acidic brine. As a result, pH values cover a small range, with almost all the pores having a pH of 2.9, that of the incoming acidic brine. With a medium flow velocity, the residence time is large enough to sustain a lower hydrogen ion concentration in and near reactive pores. The hydrogen ion concentrations span almost an order of magnitude, with much larger pH values in reactive pores than those in non-reactive pores. Although not shown here, simulation results show that with a low flow velocity, for example, 2.3×10^{-5} cm/s, the concentration field becomes relatively homogeneous again, except with most pores having low hydrogen ion concentrations and high pH values. Under this condition, diffusion is faster than advection and becomes the dominant transport process, which homogenizes the concentrations in reactive and non-reactive pores. Corresponding to the relatively homogeneous concentration fields with high and low flow velocities, differences between R_N and R_N' are relatively small.

DISCUSSION

Our modeling results have shown that under the conditions studied here, pore-to-pore heterogeneities in the mineralogy of the solid phase can generate large spatial variations in aqueous concentrations. Averaged concentrations, by representing the reaction progress using single concentration values, may not adequately capture

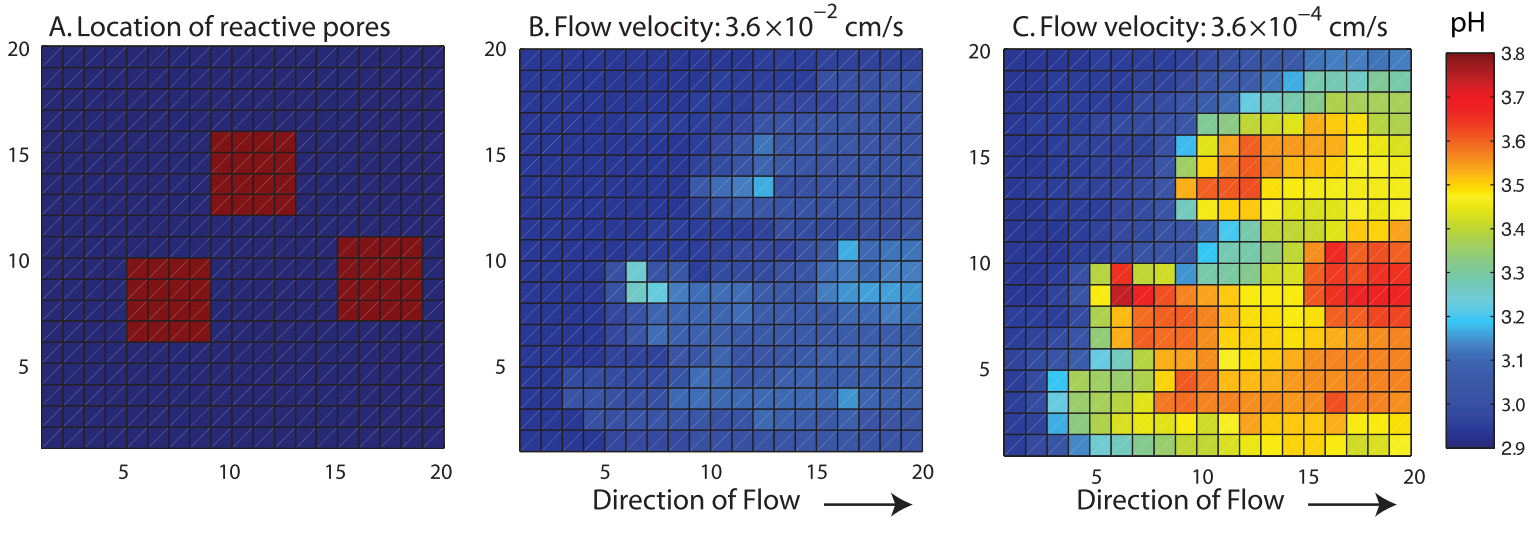

Fig. 8. (A) The distribution of reactive minerals (in red) in the middle layer of a network with reactive clusters of four pores in length and total reactive mineral abundance of 12.5%; (B) and (C) Steady-state pH fields for two different mean flow velocities. The steady-state $\log_{10}[Ca^{2+}]$ fields look very similar to those of pH.

the effects of these spatial variations in concentrations. As a result, over the length scale of several millimeters, reaction rates determined from the averaged concentrations can overestimate the anorthite dissolution by a factor of three. Under the thermodynamic conditions established by the dissolution of anorthite, kaolinite would precipitate but an averaging calculation would erroneously predict its dissolution. This is because averaged concentrations indiscriminately average over all pores, while the overall reaction rates depend *only* on concentrations in pores that contain reactive minerals. Analogously, concentrations measured from field sampling of waters from heterogeneous formations, essentially the averaged concentrations, may not accurately reflect reaction progress and may therefore provide erroneous information on reaction rates.

The applicability of averaged concentrations in determining reaction rates in porous media largely depends on the mineralogical and hydrodynamic conditions that can affect the spatial variability of concentrations. With abundant reactive minerals, the concentrations in non-reactive pores are largely influenced by those in reactive pores and the averaged concentrations are more applicable than otherwise. Reactive minerals that are evenly distributed in small clusters facilitate mass transport between reactive and non-reactive pores, reduce concentration heterogeneities, and lead to a better representation of reaction progress by the averaged concentrations. Moreover, with high or low flow velocities, the relative dominance of advection or diffusion results in relatively small differences between concentrations in reactive and non-reactive pores, and favors the applicability of averaged concentrations. It is under the medium flow conditions that the spatial variations in concentrations develop to their extreme. The applicability also depends on the type of reaction, especially the form of reaction rate laws. With highly nonlinear rate laws, such as that for the kaolinite reaction, even small errors introduced in the averaged concentrations can lead to large errors in reaction rate prediction, to an extent that the kaolinite reaction direction can not be correctly determined.

The inapplicability of averaged concentrations in determining reaction rates in porous media under certain conditions essentially stems from the lack of complete mixing at the network scale. Such phenomena have been observed in several other studies at larger spatial scales (Kapoor and others, 1997; Raje and Kapoor, 2000; Gramling and others, 2002), albeit the incomplete mixing can be caused by different reasons, including the chemical heterogeneities of mineral location and abundance studied here, as well as flow variability (Kapoor and others, 1997). Such errors may suggest that as long as the conditions for incomplete mixing exist, the averaged concentration may not be directly applicable in reaction rates determined in lab-measured reaction kinetics, which are often measured under conditions of complete mixing. The extent of introduced errors depends on the extent of mixing.

The extent of mixing also depends on the relative rates of flow, diffusion or dispersion, and reaction processes, which in term depend on the time scales of individual processes and the characteristic length of the study domain. In this work, we focus on a pore network of several millimeters in length and we found a threshold flow rate of 10^{-5} cm/s for the diffusion to become the dominant transport process to homogenize the concentration fields. Flow rates slower than that would homogenize the concentration fields and there would be no significant scaling effects. The characteristic time scale of diffusion or dispersion is proportional to the square of the characteristic length scale (L^2/D), while the time scale of advection is directly proportional to the characteristic length scale (L/v). As a result, the time scale required for the diffusion or dispersion to homogenize the concentration field increases much faster than the time scale of advection. As such, at a longer length scale, the threshold flow rate can become much smaller than 10^{-5} cm/s. This implies that

even for systems such as soil and saprolite where flow rates are much smaller, the condition of incomplete mixing can still arise when the characteristic length is long enough. Under such conditions, the use of field-measured concentrations can still introduce errors in determining reaction rates. Similarly, at a longer length scale, even with the same reaction rates, large concentration gradients can develop due to the longer residence time, and scaling effects can still become significant.

These findings have potentially important implications for the interpretation of field data. The results suggest that measured concentrations from field samples of formation waters, as an analog of averaged concentrations, can be misleading in determining reaction rates in heterogeneous porous media under conditions where reactive minerals only occupy a small percentage of the solid phase and are clustered together. Underestimation or overestimation of reaction rates results in overestimation or underestimation, respectively, of time scales required for processes such as CO_2-mediated mineral weathering. The prediction of wrong reaction directions provides incorrect hydrogeological properties of subsurface systems, and may lead to erroneous predictions in the changes of porosity and permeability of subsurface formations. Models calibrated using such data may produce erroneous conclusions. One such example may be the often-observed lab-field chemical weathering rate discrepancy: the field-measured reaction rates are often orders of magnitude smaller than the measurement in the lab system (White and Brantley, 2003). For the anorthite dissolution rates, we found a rate discrepancy on the order of a factor of 3, which is much smaller than the observed orders of magnitude difference. Partly this may be due to the fact that in the field, all possible contributing factors, including the age of reacting minerals, contact area between flowing water and surface, and physical and chemical heterogeneities, comes into play, while in the work, we really only focus on the effects of chemical heterogeneities.

Although the averaged concentrations can introduce large errors in predicting reaction rates when directly used in lab-measured mineral dissolution and precipitation reaction kinetics, practically they are the only concentrations that can be measured, because it is not feasible, and probably not possible, to measure concentrations in individual pores. As such, upscaled reaction rate laws need to be developed to provide means of taking into account the small scale variations in mineralogy and pore structure in order to accurately infer reaction rates from averaged concentrations.

ACKNOWLEDGMENTS

The authors acknowledge the financial support by Department of Energy, Office of Basic Energy Sciences, through Grant No. DE-FG02-05ER15636. Support from BP and Ford Motor Company through the Carbon Mitigation Initiative at Princeton University is also greatly appreciated. The authors thank Carl I. Steefel and two anonymous reviewers for their constructive comments that have significantly improved the paper.

References

Alekseyev, V. A., Medvedeva, L. S., Prisyagina, N. I., Meshalkin, S. S., and Balabin, A. I., 1997, Change in the dissolution rates of alkali feldspars as a result of secondary mineral precipitation and approach to equilibrium: Geochimica et Cosmochimica Acta, v. 61, p. 1125-1142.

Anbeek, C., 1993, The Effect of Natural Weathering on Dissolution Rates: Geochimica et Cosmochimica Acta, v. 57, p. 4963-4975.

Anderson, R. T., Vrionis, H. A., Ortiz-Bernad, I., Resch, C. T., Long, P. E., Dayvault, R., Karp, K., Marutzky, S., Metzler, D. R., Peacock, A., White, D. C., Lowe, M., and Lovley, D. R., 2003, Stimulating the *in situ* activity of Geobacter species to remove uranium from the groundwater of a uranium-contaminated aquifer: Applied and Environmental Microbiology, v. 69, p. 5884-5891.

Appelo, C. A. J., and Postma, D., 1996, Geochemistry, groundwater and pollution: Rotterdam, A. A. Balkema, 536 p.

Bear, J., 1972, Dynamics of Fluids in Porous media: New York, Dover Publications, Inc., 764 p.
Berner, R. A., Lasaga, A. C., and Garrels, R. M., 1983, The carbonate-silicate geochemical cycle and its effect on atmospheric carbon dioxide over the past 100 million years: American Journal of Science, v. 283, p. 641-683.
Blunt, M. J., 2001, Flow in porous media - pore-network models and multiphase flow: Current Opinion in Colloid and Interface Science, v. 6, p. 197-207.
Borgia, G. C., Brown, R. J. S., and Fantazzini, P., 1996, Nuclear magnetic resonance relaxivity and surface-to-volume ratio in porous media with a wide distribution of pore sizes: Journal of Applied Physics, v. 79, p. 3656-3664.
Brantley, S. L., and Velbel, M. A., 1993, Preface: Chemical Geology, v. 105, p. VII-IX.
Carozzi, A. V., 1993, Sedimentary petrography: Sedimentary Geology series: Englewood Cliffs, New Jersey, PTR Prentice Hall, 263 p.
Casey, W. H., Banfield, J. F., Westrich, H. R., and McLaughlin, L., 1993, What do dissolution experiments tell us about natural weathering?: Chemical Geology, v. 105, p. 1-15.
Celia, M. A., Reeves, P. C., and Ferrand, L. A., 1995, Recent Advances in Pore Scale Models for Multiphase Flow in Porous-Media: Reviews of Geophysics, v. 33, p. 1049-1057.
Duan, Z., and Sun, R., 2003, An improved model calculating CO_2 solubility in pure water and aqueous NaCl solutions from 273 to 533 K and from 0 to 2000 bar: Chemical Geology, v. 193, p. 257-271.
Freeze, R. A., 1975, A stochastic-conceptual analysis of one-dimensional groundwater flow in nonuniform homogeneous media: Water Resources Research, v. 11, p. 725-741.
Frosch, G. P., Tillich, J. E., Haselmeier, R., Holz, M., and Althaus, E., 2000, Probing the pore space of geothermal reservoir sandstones by Nuclear Magnetic Resonance: Geothermics, v. 29, p. 671-687.
Ganor, J., Mogollon, J. L., and Lasaga, A. C., 1995, The Effect of pH on Kaolinite Dissolution Rates and on Activation-Energy: Geochimica et Cosmochimica Acta, v. 59, p. 1037-1052.
Gaus, I., Azaroual, M., and Czernichowski-Lauriol, I., 2005, Reactive transport modeling of the impact of CO_2 injection on the clayey cap rock at Sleipner (North Sea): Chemical Geology, v. 217, p. 319-337.
Giambalvo, E. R., Steefel, C. I., Fisher, A. T., Rosenberg, N. D., and Wheat, C. G., 2002, Effect of fluid-sediment reaction on hydrothermal fluxes of major elements, eastern flank of the Juan de Fuca Ridge: Geochimica et Cosmochimica Acta, v. 66, p. 1739-1757.
Giammar, D. E., Bruant, R. G., and Peters, C. A., 2005, Forsterite dissolution and magnesite precipitation at conditions relevant for deep saline aquifer storage and sequestration of carbon dioxide: Chemical Geology, v. 217, p. 257-276.
Gramling, C. M., Harvey, C. F., and Meigs, L. C., 2002, Reactive transport in porous media: A comparison of model prediction with laboratory visualization: Environmental Science and Technology, v. 36, p. 2508-2514.
Jia, C., Shing, K., and Yortsos, Y. C., 1999, Visualization and simulation of non-aqueous phase liquids solubilization in pore networks: Journal of Contaminant Hydrology, v. 35, p. 363-387.
Johnson, J. W., Oelkers, E. H., and Helgeson, H. C., 1992, SUPCRT92: a software package for calculating the standard molal thermodynamic properties of minerals, gases, aqueous species, and reactions from 1 to 5000 bar and 0 to 1000 deg C: Computers and Geosciences, v. 18, p. 899-947.
Kapoor, V., Gelhar, L. W., and MirallesWilhelm, F., 1997, Bimolecular second-order reactions in spatially varying flows: Segregation induced scale-dependent transformation rates: Water Resources Research, v. 33, p. 527-536.
Kapoor, V., Jafvert, C. T., and Lyn, D. A., 1998, Experimental study of a bimolecular reaction in Poiseuille flow: Water Resources Research, v. 34, p. 1997-2004.
Knapp, R. B., 1989, Spatial and temporal scales of local equilibrium in dynamic fluid-rock systems: Geochimica et Cosmochimica Acta, v. 53, p. 1955-1964.
Kump, L. R., Brantley, S. L., and Arthur, M. A., 2000, Chemical weathering, atmospheric CO_2, and climate: Annual Review of Earth and Planetary Science, v. 28, p. 611 - 667.
Lasaga, A. C., 1998, Kinetic theory in the earth sciences: Princeton series in geochemistry: Princeton, Princeton University Press, 811 p.
Li, L., Peters, C. A., and Celia, M. A., 2006, Upscaling geochemical reaction rates using pore-scale network modeling: Advances in Water Resources, v. 29, p. 1351-1370.
——— 2007a, Reply to "Comment on upscaling geochemical reaction rates using pore-scale network modeling" by Peter C. Lichtner and Qinjun Kang: Advances in Water Resources, v. 30, p. 691-695.
——— 2007b, Effects of mineral spatial distribution on reaction rates in porous media: Water Resources Research, v. 43, W01419, doi:10.1029/2005WR004848.
Lichtner, P. C., 1985, Continuum Model for Simultaneous Chemical-Reactions and Mass- Transport in Hydrothermal Systems: Geochimica et Cosmochimica Acta, v. 49, p. 779-800.
Lindquist, W. B., Venkatarangan, A., Dunsmuir, J., and Wong, T. F., 2000, Pore and throat size distributions measured from synchrotron X- ray tomographic images of Fontainebleau sandstones: Journal of Geophysical Research-Solid Earth, v. 105, p. 21509-21527.
Lymberopoulos, D. P., and Payatakes, A. C., 1992, Derivation of Topological, Geometrical, and Correlational Properties of Porous-Media from Pore-Chart Analysis of Serial Section Data: Journal of Colloid and Interface Science, v. 150, p. 61-80.
Maher, K., DePaolo, D. J., and Lin, J. C. F., 2004, Rates of silicate dissolution in deep-sea sediment: *In situ* measurement using U-234/U-238 of pore fluids: Geochimica et Cosmochimica Acta, v. 68, p. 4629-4648.
Malmstrom, M. E., Destouni, G., Banwart, S. A., and Stromberg, B. H. E., 2000, Resolving the Scale-Dependence of Mineral Weathering Rates: Environmental Science and Technology, v. 34, p. 1375-1378.
Malmstrom, M. E., Destouni, G., and Martinet, P., 2004, Modeling expected solute concentration in randomly heterogeneous flow systems with multicomponent reactions: Environmental Science and Technology, v. 38, p. 2673-2679.

Martin-Hayden, J. M., and Robbins, G. A., 1997, Plume distortion and apparent attenuation due to concentration averaging in monitoring wells: Ground Water, v. 35, p. 339-346.
Meile, C., and Tuncay, K., 2006, Scale dependence of reaction rates in porous media: Advances in Water Resources, v. 29, p. 62-71.
Mo, Z., and Friedly, J. C., 2000, Local reaction and diffusion in porous media transport models: Water Resources Research, v. 36, p. 431-438.
Molz, F. J., and Widdowson, M. A., 1988, Internal Inconsistencies in Dispersion-Dominated Models That Incorporate Chemical and Microbial Kinetics: Water Resources Research, v. 24, p. 615-619.
Morel, F., and Hering, J. G., 1993, Principles and Applications of Aquatic Chemistry: New York, Wiley, xv, 588 p.
Nagy, K. L., Blum, A. E., and Lasaga, A. C., 1991, Dissolution and Precipitation Kinetics of Kaolinite at 80-Degrees-C and pH 3 - the Dependence on Solution Saturation State: American Journal of Science, v. 291, p. 649-686.
Newman, J. S., 1991, Electrochemical systems: New Jersey, Prentice Hall, 672 p.
Oelkers, E. H., and Schott, J., 1995, Experimental study of anorthite dissolution and the relative mechanism of feldspar hydrolysis: Geochimica et Cosmochimica Acta, v. 59, p. 5039-5053.
Parkhurst, D. L., and Plummer, L. N., 1993, Geochemical models, *in* Alley, W. M., editor, Regional Groundwater Quality: New York, Van Nostrand Reinhold, p. 199-225.
Parnell, J., and Roderic A., 1993, Hydrologic control of chemical disequilibria in soil and surface waters, Sogndal, Norway: Chemical Geology, v. 105, p. 101-115.
Plummer, L. N., Parkhurst, D. L., and Thorstenson, D. C., 1983, Development of Reaction Models for Groundwater Systems: Geochimica et Cosmochimica Acta, v. 47, p. 665-685.
Postma, D., 1990, Kinetics of Nitrate Reduction by Detrital Fe(II)-Silicates: Geochimica et Cosmochimica Acta, v. 54, p. 903-908.
Postma, D., Boesen, C., Kristiansen, H., and Larsen, F., 1991, Nitrate Reduction in an Unconfined Sandy Aquifer - Water Chemistry, Reduction Processes, and Geochemical Modeling: Water Resources Research, v. 27, p. 2027-2045.
Prat, M., 2002, Recent advances in pore-scale models for drying of porous media: Chemical Engineering Journal, v. 86, p. 153-164.
Raje, D. S., and Kapoor, V., 2000, Experimental study of bimolecular reaction kinetics in porous media: Environmental Science and Technology, v. 34, p. 1234-1239.
Ross, S. M., 2000, Introduction to Probability Models: San Diego, California, Academic Press, xv, 693 p.
Sen, P. N., Straley, C., Kenyon, W. E., and Wittingham, M. S., 1990, Surface-to-volume ratio, charge density, nuclear magnetic relaxation, and permeability in clay-bearing sandstones: Geophysics, v. 55, p. 61-69.
Stark, J., and Manga, M., 2000, The motion of long bubbles in a network of tubes: Transport in Porous Media, v. 40, p. 201-218.
Steefel, C. I., and Van Cappellen, P., 1990, A new kinetic approach to modeling water-rock interaction: the role of nucleation, precursors, and Ostwald ripening: Geochimica et Cosmochimica Acta, v. 54, p. 2657-2677.
Suchomel, B. J., Chen, B. M., and Allen, M. B., 1998, Macroscale properties of porous media from a network model of biofilm processes: Transport in Porous Media, v. 31, p. 39-66.
Swoboda-Colberg, N. G., and Drever, J. I., 1993, Mineral dissolution rates in plot-scale field and laboratory experiments: Chemical Geology, v. 105, p. 51-69.
Turcke, M. A., and Kueper, B. H., 1996, Geostatistical analysis of the Borden aquifer hydraulic conductivity field: Journal of Hydrology, v. 178, p. 223-240.
Velbel, M. A., 1993, Constancy of silicate-mineral weathering-rate ratios between natural and experimental weathering: implications for hydrologic control of differences in absolute rates: Chemical Geology, v. 105, p. 89-99.
Walker, J. C. G., Hays, P. B., and Kasting, J. F., 1981, A negative feedback mechanism for the long term stabilization of Earth's surface temperatures: Journal of Geophysical Research-Solid Earth, v. 86, p. 9776-9782.
Wardlaw, N. C., Li, Y., and Forbes, D., 1987, Pore-Throat Size Correlation from Capillary-Pressure Curves: Transport in Porous Media, v. 2, p. 597-614.
White, A. F., 1995, Chemical weathering rates of silicate minerals in soils, *in* White, A. F., and Brantley, S. L., editors, Chemical Weathering Rates of Silicate Minerals: Washington, D.C., Mineralogical Society of America, Reviews in Mineralogy, v. 31, p. 407-461.
White, A. F., and Brantley, S. L., 1995, Chemical weathering rates of silicate minerals: An overview, *in* White, A. F., and Brantley, S. L., editors, Chemical Weathering Rates of Silicate Minerals: Washington, D. C., Mineralogical Society of America, Reviews in Mineralogy, v. 31, p. 1-22.
——— 2003, The effect of time on the weathering of silicate minerals: why do weathering rates differ in the laboratory and field?: Chemical Geology, v. 202, p. 479-506.
White, A. F., Blum, A. E., Schulz, M. S., Vivit, D. V., Stonestrom, D. A., Larsen, M., Murphy, S. F., and Eberl, D., 1998, Chemical weathering in a tropical watershed, Luquillo mountains, Puerto Rico: I. Long-term versus short-term weathering fluxes: Geochimica et Cosmochimica Acta, v. 62, p. 209-226.
White, S. P., Allis, R. G., Chidsey, T., Morgan, C., Gwynn, W., Moore, J., and Adams, M., 2005, Simulation of reactive transport of injected CO_2 on the Colorado Plateau, Utah, USA: Chemical Geology, v. 217, p. 387-405.
Yang, Y. S., Cronin, A. A., Elliot, T., and Kalin, R. M., 2004, Characterizing a heterogeneous hydrogeological system using groundwater flow and geochemical modeling: Journal of Hydraulic Research, v. 42, p. 147-155.

Zachara, J. M., Kukkadapu, R. K., Gassman, P. L., Dohnalkova, A., Fredrickson, J. K., and Anderson, T., 2004, Biogeochemical transformation of Fe minerals in a petroleum-contaminated aquifer: Geochimica et Cosmochimica Acta, v. 68, p. 1791-1805.

Zhu, C., 2005, *In situ* feldspar dissolution rates in an aquifer: Geochimica et Cosmochimica Acta, v. 69, p. 1435-1453.